

Thermal dehydration of calcium sulfate dihydrate: Physico-geometrical kinetic modeling and influence of self-generated water vapor

Shun Iwasaki and Nobuyoshi Koga*

Department of Science Education, Graduate School of Education, Hiroshima University, 1-1-1 Kagamiyama, Higashi-Hiroshima 739-8524, Japan

Contents

S1. Sample Characterization.....	s2
Figure S1. SEM images of CaSO ₄ ·2H ₂ O sample particles with different magnifications: (a) ×1,000, (b) ×3,000, (c) ×5,000, and (d) ×10,000.....	s2
Figure S2. Powder XRD pattern of CaSO ₄ ·2H ₂ O sample.....	s2
Figure S3. FT-IR spectrum of CaSO ₄ ·2H ₂ O sample.....	s3
Table S1. Assignments of IR absorption peaks for the original sample. ⁵²⁻⁵⁴	s3
S2. Thermal Dehydration Behaviors.....	s3
Figure S4. TG/DTA–MS curves for the CaSO ₄ ·2H ₂ O sample: (a) TG–DTA curves and (b) MS ion thermograms of <i>m/z</i> = 18, 17, and 16.....	s3
Figure S5. Changes in the XRD pattern during heating the CaSO ₄ ·2H ₂ O sample in a stream of dry N ₂ gas (100 cm ³ min ⁻¹): (a) according to the stepwise isothermal heating program, (b) according to isothermal heating at 373 K, and (c) XRD pattern of the product solid.....	s3
Figure S6. Change in the crystallite size of γ-CaSO ₄ produced by the thermal dehydration of the CaSO ₄ ·2H ₂ O sample under the open atmosphere conditions in a stream of dry N ₂ gas (100 cm ³ min ⁻¹): (a) with temperature during the stepwise isothermal heating and (b) with time during the isothermal heating at 373 K.....	s4
S3. Thermal Dehydration in Inert Gas Atmosphere.....	s4
(1) Kinetic data measurements.....	s4
Figure S7. TG–DTG curves for the thermal dehydration of CaSO ₄ ·2H ₂ O (<i>m</i> ₀ = 5.033 ± 0.022 mg) under the open-atmosphere conditions in a stream of dry N ₂ gas (flow rate: 80 cm ³ min ⁻¹), recorded under linear nonisothermal conditions at different β values in the range of 0.5–10 K min ⁻¹	s4
Figure S8. TG–DTG curves for the thermal dehydration of CaSO ₄ ·2H ₂ O (<i>m</i> ₀ = 5.000 ± 0.021 mg) under the open-atmosphere conditions in a stream of dry N ₂ gas (flow rate: 80 cm ³ min ⁻¹), recorded under CRTA conditions at various <i>C</i> values in the range of 5.0–15.0 μg min ⁻¹ : (a) typical TG–DTG records and (b) temperature profile and transformation rate at various programmed <i>C</i> values.....	s4
(2) Isoconversional kinetic analysis.....	s5
Figure S9. Friedman plots at various α values from 0.1 to 0.9 in steps of 0.1 for the thermal dehydration of CaSO ₄ ·2H ₂ O to CaSO ₄ under the open-atmosphere conditions in a stream of dry N ₂ gas in three different temperature regions: (a) low-, (b) middle-, and (c) high-temperature regions.....	s5
Figure S10. Results of Friedman plots applied to the kinetic data of the entire temperature range for the thermal dehydration of CaSO ₄ ·2H ₂ O to CaSO ₄ under the open-atmosphere conditions in a stream of dry N ₂ gas: (a) Friedman plots at various α values from 0.1 to 0.9 in steps of 0.1 and (b) <i>E</i> _a values at various α values.....	s5
(3) Effect of sample mass.....	s5
Figure S11. Influence of sample mass (<i>m</i> ₀) on the TG–DTG curves for the thermal dehydration of CaSO ₄ ·2H ₂ O recorded under the open-atmosphere conditions in a stream of dry N ₂ gas.....	s5
(4) Kinetic analysis based on IP–SR–PBR models.....	s5
Table S2. Differential kinetic equations for IP–SR–PBR(<i>n</i>) models.....	s6
Table S3. Optimized <i>k</i> _{IP} (=1/ <i>t</i> _{IP}), <i>k</i> _{SR} , and <i>k</i> _{PBR(2)} values for the thermal dehydration of CaSO ₄ ·2H ₂ O to CaSO ₄ under the open-atmosphere conditions in a stream of dry N ₂ gas.....	s6
S4. Thermal Dehydration in Self-Generated Atmosphere.....	s7
(1) Effect of sample mass.....	s7
Figure S12. Influence of sample mass (<i>m</i> ₀) on the TG–DTG curves for the thermal dehydration of CaSO ₄ ·2H ₂ O recorded under the semi-closed conditions in a stream of N ₂ gas.....	s7

* Corresponding author. E-mail: nkoga@hiroshima-u.ac.jp

(2) Kinetic data measurements.....	s7
Figure S13. TG–DTG curves under CRTA conditions for the thermal dehydration of approximately 15.0 mg of $\text{CaSO}_4 \cdot 2\text{H}_2\text{O}$ (approximately 15.0 mg) under the semi-closed conditions in a stream of N_2 gas (flowrate: $80 \text{ cm}^3 \text{ min}^{-1}$): (a) typical TG–DTG records and (b) temperature profile and transformation rate at various programmed C values.....	s7
(3) Isoconversional kinetic analysis.....	s7
Figure S14. Isoconversional kinetic analysis for the thermal dehydration of $\text{CaSO}_4 \cdot 2\text{H}_2\text{O}$ recorded under CRTA conditions and semi-closed conditions in a stream of dry N_2 gas: (a) Friedman plots at different α values, (b) E_a values at different α values, and (c) experimental master plot of $(d\alpha/d\theta)$ versus α	s7
(4) Morphological changes.....	s8
Figure S15. SEM images of the sample dehydrated partially to different α values by heating nonisothermally at a β value of 3 K min^{-1} under the same conditions as those for the kinetic data measurements for the $\text{CaSO}_4 \cdot 2\text{H}_2\text{O}$ (approximately 15.0 mg) under the semi-closed conditions: (a) $\alpha = 0.01$ (370 K), (b) $\alpha = 0.04$ (390 K), (c) $\alpha = 0.13$ (403 K), (d) $\alpha = 0.53$ (420 K), (e) $\alpha = 0.81$ (430 K), (f) $\alpha = 0.98$ (443 K), and (g) $\alpha = 0.99$ (480 K).....	s8
(5) Mathematical deconvolution analysis.....	s8
Figure S16. Typical results of MDA for the DTG peaks of the thermal dehydration of $\text{CaSO}_4 \cdot 2\text{H}_2\text{O}$ under the semi-closed conditions: (a) at a constant temperature of 391 K (lower temperature) and (b) at a β of 3 K min^{-1} (higher temperature).....	s8
Table S4. Results of kinetic analysis for the component reaction steps using MDA for the thermal dehydration of $\text{CaSO}_4 \cdot 2\text{H}_2\text{O}$ under the semi-closed conditions.....	s9
Figure S17. Series of kinetic curves for each reaction step i at different constant temperatures in the lower-temperature region, as obtained by MDA: (a) $i = 1$, (b) $i = 2$, and (c) $i = 3$	s10
Figure S18. Series of kinetic curves for each reaction step i at different β values in the higher-temperature region, as obtained by MDA: (a) $i = 1$, (b) $i = 2$, and (c) $i = 3$	s10
Figure S19. Friedman plots at various α_i values for the mathematically separated kinetic data at various constant temperatures in the lower-temperature region: (a) $i = 1$, (b) $i = 2$, and (c) $i = 3$	s11
Figure S20. Results of the isoconversional kinetic analysis applied to the mathematically separated kinetic data at various constant temperatures in the lower-temperature region: (a) E_a values at various α_i values and (b) experimental master plots of $d\alpha_i/d\theta_i$ versus α_i	s11
Figure S21. Friedman plots at various α_i values for the mathematically separated kinetic data at various β values in the higher-temperature region: (a) $i = 1$, (b) $i = 2$, and (c) $i = 3$	s12
Figure S22. Results of the isoconversional kinetic analysis applied to the mathematically separated kinetic data at various β values in the higher-temperature region: (a) E_a values at various α_i values and (b) experimental master plots of $d\alpha_i/d\theta_i$ versus α_i	s12

S1. Sample Characterization

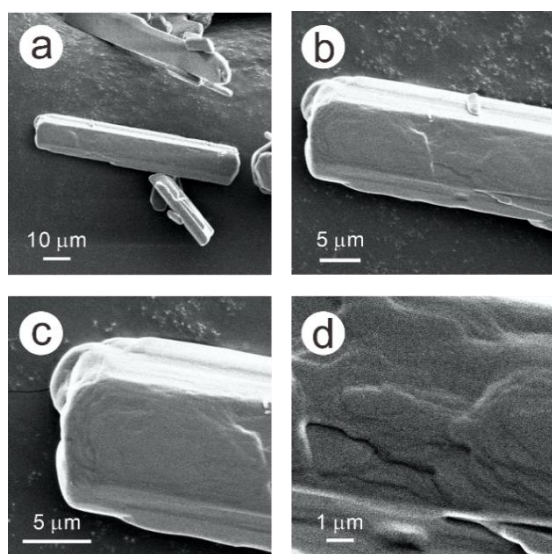


Figure S1. SEM images of $\text{CaSO}_4 \cdot 2\text{H}_2\text{O}$ sample particles with different magnifications: (a) $\times 1,000$, (b) $\times 3,000$, (c) $\times 5,000$, and (d) $\times 10,000$.

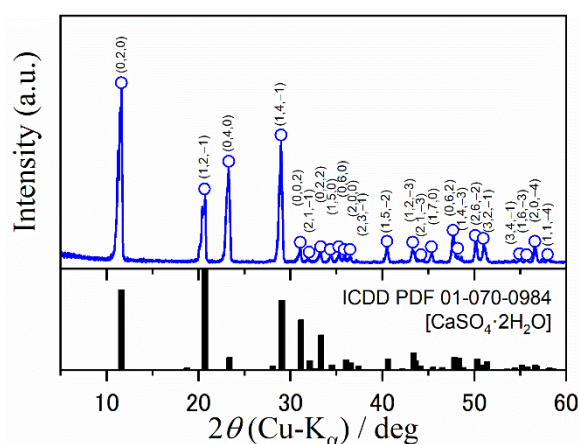


Figure S2. Powder XRD pattern of $\text{CaSO}_4 \cdot 2\text{H}_2\text{O}$ sample.

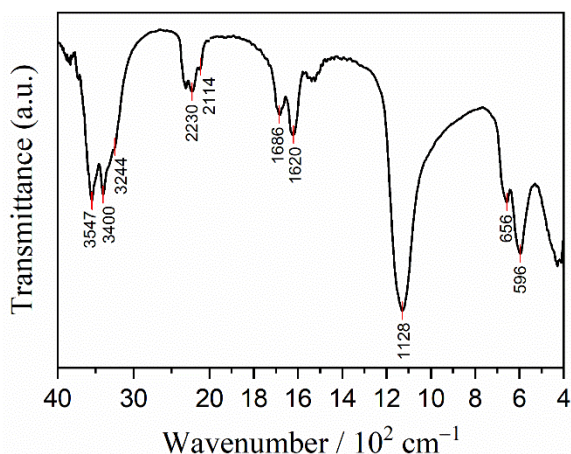


Figure S3. FT-IR spectrum of $\text{CaSO}_4 \cdot 2\text{H}_2\text{O}$ sample.

Table S1. Assignments of IR absorption peaks for the original sample.⁵²⁻⁵⁴

Peak position / cm^{-1}	Vibration mode
3547, 3400, and 3244	O–H stretching vibration
2230 and 2114	overtones of SO_4^{2-}
1686 and 1620	O–H–O bending vibration
1128	S–O stretching vibration
656 and 596	SO_4^{2-} antisymmetric band

S2. Thermal Dehydration Behaviors

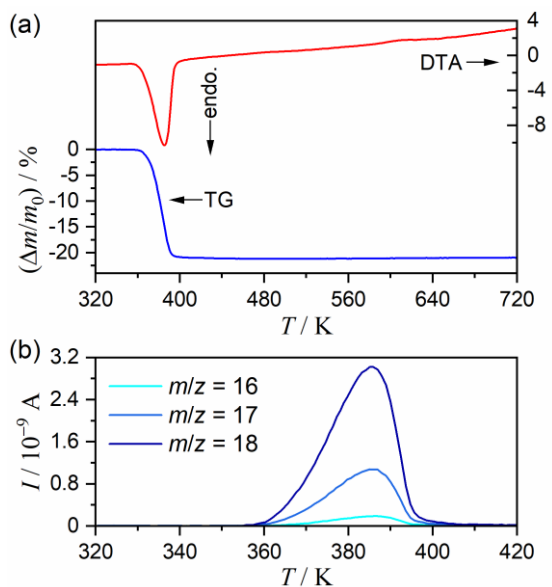


Figure S4. TG/DTA–MS curves for the $\text{CaSO}_4 \cdot 2\text{H}_2\text{O}$ sample: (a) TG–DTA curves and (b) MS ion thermograms of $m/z = 18, 17,$ and 16 .

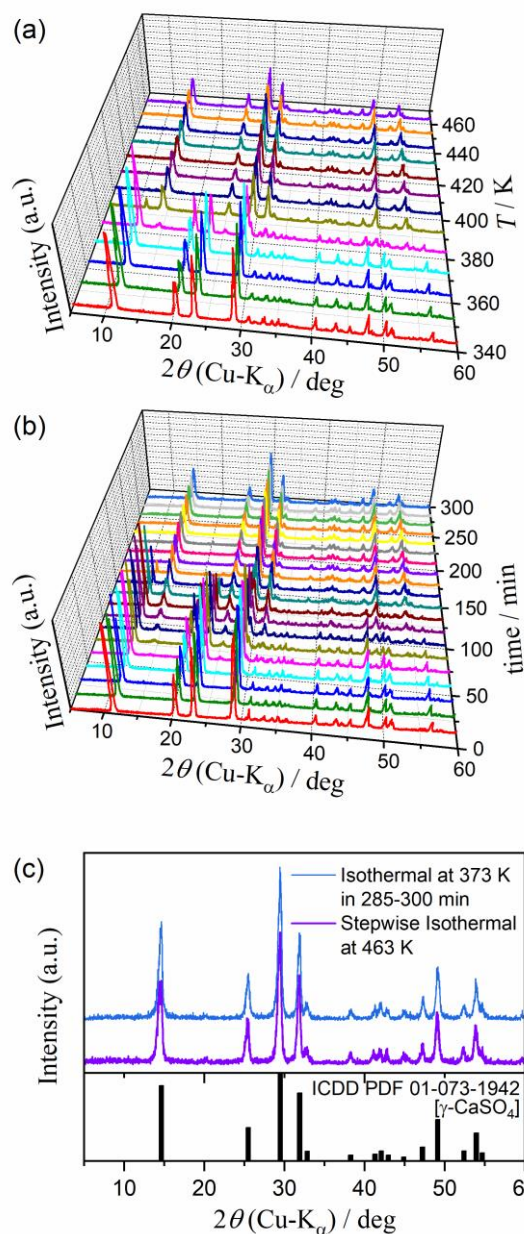


Figure S5. Changes in the XRD pattern during heating the $\text{CaSO}_4 \cdot 2\text{H}_2\text{O}$ sample in a stream of dry N_2 gas ($100 \text{ cm}^3 \text{ min}^{-1}$): (a) according to the stepwise isothermal heating program, (b) according to isothermal heating at 373 K , and (c) XRD pattern of the product solid.

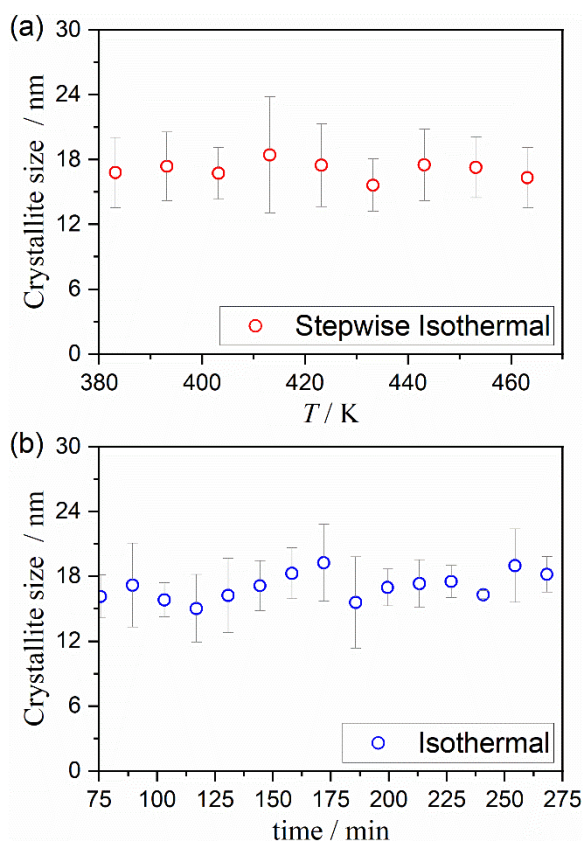


Figure S6. Change in the crystallite size of γ -CaSO₄ produced by the thermal dehydration of the CaSO₄·2H₂O sample under the open-atmosphere conditions in a stream of dry N₂ gas (100 cm³ min⁻¹): (a) with temperature during the stepwise isothermal heating and (b) with time during the isothermal heating at 373 K.

S3. Thermal Dehydration in Inert Gas Atmosphere

(1) Kinetic data measurements

Figure S7 shows the TG–DTG curves for the thermal dehydration of CaSO₄·2H₂O in a stream of dry N₂ gas, recorded under linear nonisothermal conditions at different β values. TG–DTG curves indicate a smooth mass-loss process to form anhydride without any indication of formation of intermediate hydrates and shift systematically to higher temperatures with increasing β . The smooth mass-loss process is also confirmed by the measurements conducted under the CRTA conditions, as shown in Figure S8. The linear decrease in the sample mass to anhydride is achieved by a smooth temperature change with a concaved shape characterized by the initial decrease and final increase in the sample temperature after exhibiting the minimum midway through the mass-loss process (Figure S8(a)). The initial temperature drop is attributed to the partial overshooting of the controlled transformation rate, indicating a rapid acceleration of the mass-loss process in the beginning of the process. The significant induction period for the mass-loss process observed

under isothermal conditions explains the cause of the overshooting of the sample temperature. The temperature profile during the thermal dehydration shifts systematically to higher temperatures with increasing C value (Figure S8(b)).

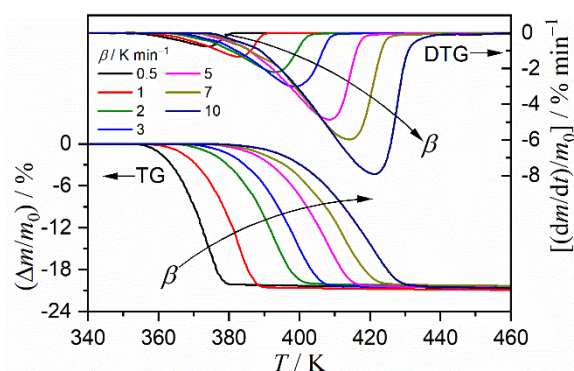


Figure S7. TG–DTG curves for the thermal dehydration of CaSO₄·2H₂O ($m_0 = 5.033 \pm 0.022$ mg) under the open-atmosphere conditions in a stream of dry N₂ gas (flowrate: 80 cm³ min⁻¹), recorded under linear nonisothermal conditions at different β values in the range of 0.5–10 K min⁻¹.

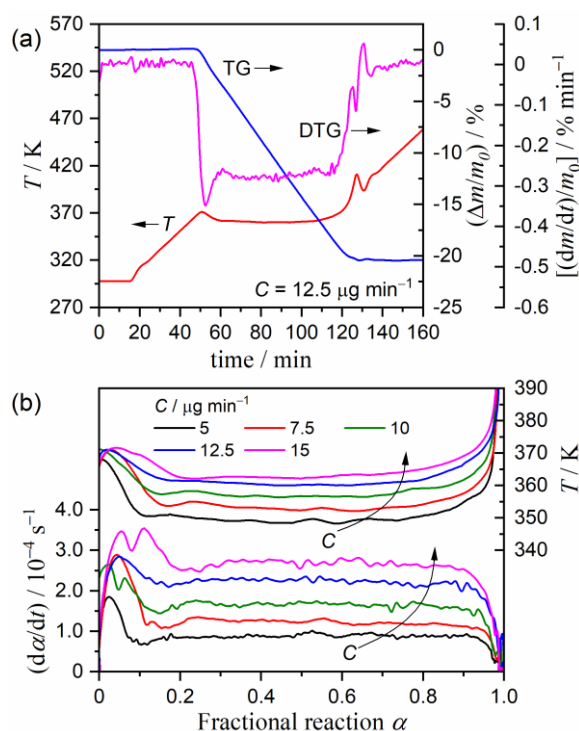


Figure S8. TG–DTG curves for the thermal dehydration of CaSO₄·2H₂O ($m_0 = 5.000 \pm 0.021$ mg) under the open-atmosphere conditions in a stream of dry N₂ gas (flowrate: 80 cm³ min⁻¹), recorded under CRTA conditions at various C values in the range of 5.0–15.0 μg min⁻¹: (a) typical TG–DTG records and (b) temperature profile and transformation rate at various programmed C values.

(2) Isoconversional kinetic analysis

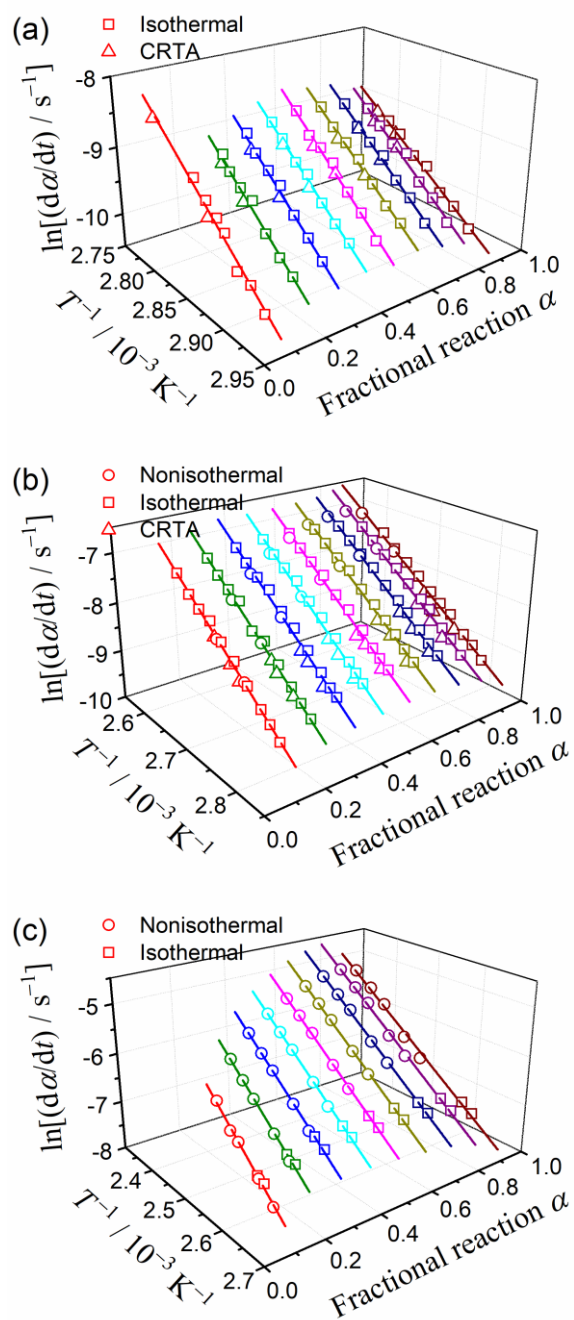


Figure S9. Friedman plots at various α values from 0.1 to 0.9 in steps of 0.1 for the thermal dehydration of $\text{CaSO}_4 \cdot 2\text{H}_2\text{O}$ to CaSO_4 under the open-atmosphere conditions in a stream of dry N_2 gas in three different temperature regions: (a) low-, (b) middle-, and (c) high-temperature regions.

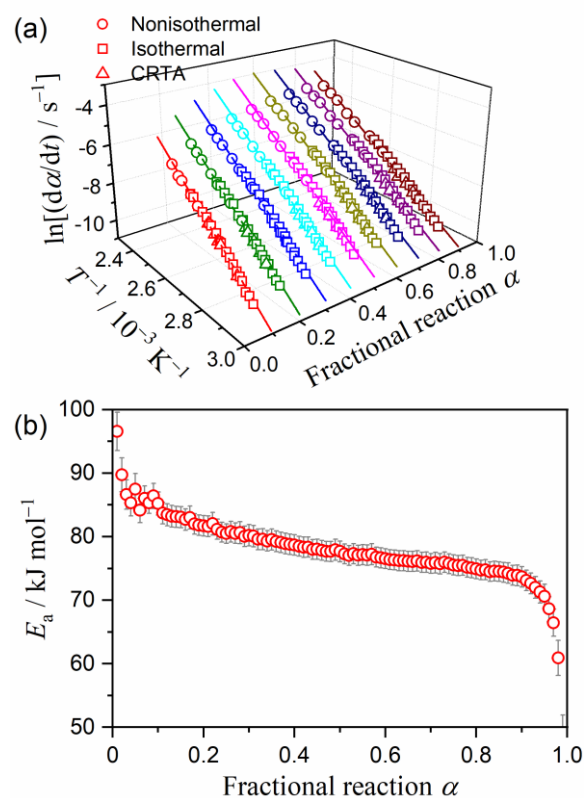


Figure S10. Results of Friedman plots applied to the kinetic data of the entire temperature range for the thermal dehydration of $\text{CaSO}_4 \cdot 2\text{H}_2\text{O}$ to CaSO_4 under the open-atmosphere conditions in a stream of dry N_2 gas: (a) Friedman plots at various α values from 0.1 to 0.9 in steps of 0.1 and (b) E_a values at various α values.

(3) Effect of sample mass

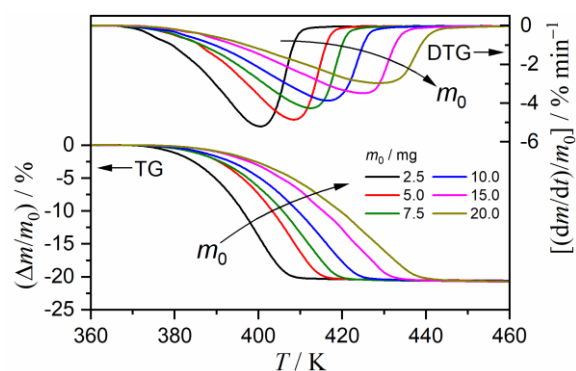


Figure S11. Influence of sample mass (m_0) on the TG-DTG curves for the thermal dehydration of $\text{CaSO}_4 \cdot 2\text{H}_2\text{O}$ recorded under the open-atmosphere conditions in a stream of dry N_2 gas.

(4) Kinetic analysis based on IP-SR-PBR models

Isothermal kinetic curves for the thermal dehydration of $\text{CaSO}_4 \cdot 2\text{H}_2\text{O}$ recorded under the open-atmosphere conditions in a stream of dry N_2 gas were subjected to kinetic modeling based on the IP-SR-PBR models (Table S2). The procedure is a nonlinear least-squares

analysis applied to each isothermal kinetic curve to determine three rate constants, namely those for the IP (k_{IP}), SR (k_{SR}), and PBR ($k_{PBR(n)}$) processes. Prior to the kinetic calculation, the initial values for k_{IP} and $k_{PBR(n)}$ were determined from the preliminary kinetic analysis for the IP process and the isoconversional kinetic analysis for the mass-loss process, respectively. After

these initial values were introduced into the kinetic equations, the initial k_{SR} value was determined graphically by comparing the experimental and calculated kinetic curves. Thereafter, the nonlinear least squares analysis was run to simultaneously optimize the k_{IP} ($=1/t_{IP}$), k_{SR} , and $k_{PBR(n)}$ values at the temperature.

Table S2. Differential kinetic equations for IP–SR–PBR(n) models

n	$\frac{d\alpha}{dt} =$
1	a) $t - t_{IP} \leq 1/k_{PBR(1)}$:
	$k_{PBR(1)}[1 - \exp(-k_{SR}(t - t_{IP}))]$
1	b) $t - t_{IP} \geq 1/k_{PBR(1)}$:
	$k_{PBR(1)}\exp(-k_{SR}(t - t_{IP})) \left[\exp\left(\frac{k_{SR}}{k_{PBR(1)}}\right) - 1 \right]$
2	a) $t - t_{IP} \leq 1/k_{PBR(2)}$:
	$-2k_{PBR(2)} \left[\left(1 + \frac{k_{PBR(2)}}{k_{SR}}\right) \exp(-k_{SR}(t - t_{IP})) + k_{PBR(2)}(t - t_{IP}) - \left(1 + \frac{k_{PBR(2)}}{k_{SR}}\right) \right]$
2	b) $t - t_{IP} \geq 1/k_{PBR(2)}$:
	$-2k_{PBR(2)}\exp(-k_{SR}(t - t_{IP})) \left[1 + \frac{k_{PBR(2)}}{k_{SR}} - \frac{k_{PBR(2)}}{k_{SR}} \exp\left(\frac{k_{SR}}{k_{PBR(2)}}\right) \right]$
3	a) $t - t_{IP} \leq 1/k_{PBR(3)}$:
	$-3k_{PBR(3)} \left[\left(1 + 2\frac{k_{PBR(3)}}{k_{SR}} + 2\left(\frac{k_{PBR(3)}}{k_{SR}}\right)^2\right) \exp(-k_{SR}(t - t_{IP})) - (-k_{PBR(3)}(t - t_{IP}))^2 + 2k_{PBR(3)}\left(\frac{k_{PBR(3)}}{k_{SR}} + 1\right)(t - t_{IP}) - \left(1 + 2\frac{k_{PBR(3)}}{k_{SR}} + 2\left(\frac{k_{PBR(3)}}{k_{SR}}\right)^2\right) \right]$
3	b) $t - t_{IP} \geq 1/k_{PBR(3)}$:
	$3k_{PBR(3)}\exp(-k_{SR}(t - t_{IP})) \left[2\left(\frac{k_{PBR(3)}}{k_{SR}}\right)^2 \left(\exp\left(\frac{k_{SR}}{k_{PBR(3)}}\right) - 1 \right) - \left(1 + 2\frac{k_{PBR(3)}}{k_{SR}}\right) \right]$

Table S3. Optimized k_{IP} ($=1/t_{IP}$), k_{SR} , and $k_{PBR(2)}$ values for the thermal dehydration of $\text{CaSO}_4 \cdot 2\text{H}_2\text{O}$ to CaSO_4 under the open-atmosphere conditions in a stream of dry N_2 gas

T / K	k_{IP} / s^{-1}	k_{SR} / s^{-1}	$k_{PBR(2)} / \text{s}^{-1}$	$R^{2,a}$	
				differential	Integral
343	1.55×10^{-4}	1.49×10^{-4}	4.10×10^{-5}	0.9702	0.9919
345	2.25×10^{-4}	1.88×10^{-4}	5.37×10^{-5}	0.9749	0.9922
347	3.75×10^{-4}	2.36×10^{-4}	6.38×10^{-5}	0.9780	0.9922
349	6.49×10^{-4}	3.16×10^{-4}	8.63×10^{-5}	0.9803	0.9936
351	7.88×10^{-4}	3.55×10^{-4}	9.80×10^{-5}	0.9791	0.9927
353	1.02×10^{-3}	4.12×10^{-4}	1.13×10^{-4}	0.9761	0.9918
355	1.40×10^{-3}	5.08×10^{-4}	1.43×10^{-4}	0.9790	0.9923
357	1.70×10^{-3}	6.38×10^{-4}	1.69×10^{-4}	0.9679	0.9910
359	2.18×10^{-3}	7.16×10^{-4}	1.98×10^{-4}	0.9746	0.9919
362	3.44×10^{-3}	9.48×10^{-4}	2.52×10^{-4}	0.9738	0.9922
365	4.83×10^{-3}	1.35×10^{-3}	3.19×10^{-4}	0.9908	0.9957
368	—	1.39×10^{-3}	3.75×10^{-4}	0.9788	0.9933
371	—	1.90×10^{-3}	5.03×10^{-4}	0.9889	0.9952
374	—	2.15×10^{-3}	5.81×10^{-4}	0.9827	0.9936
376	—	2.53×10^{-3}	6.97×10^{-4}	0.9803	0.9930
379	—	3.07×10^{-3}	8.52×10^{-4}	0.9775	0.9924
382	—	3.41×10^{-3}	9.56×10^{-4}	0.9722	0.9921

^aDetermination coefficient of the nonlinear least-squares analysis.

S4. Thermal Dehydration in Self-Generated Atmosphere

(1) Effect of sample mass

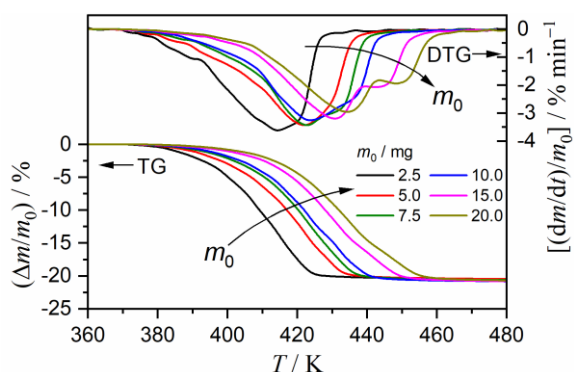


Figure S12. Influence of sample mass (m_0) on the TG–DTG curves for the thermal dehydration of $\text{CaSO}_4 \cdot 2\text{H}_2\text{O}$ recorded under the semi-closed conditions in a stream of N_2 gas.

(2) Kinetic data measurements

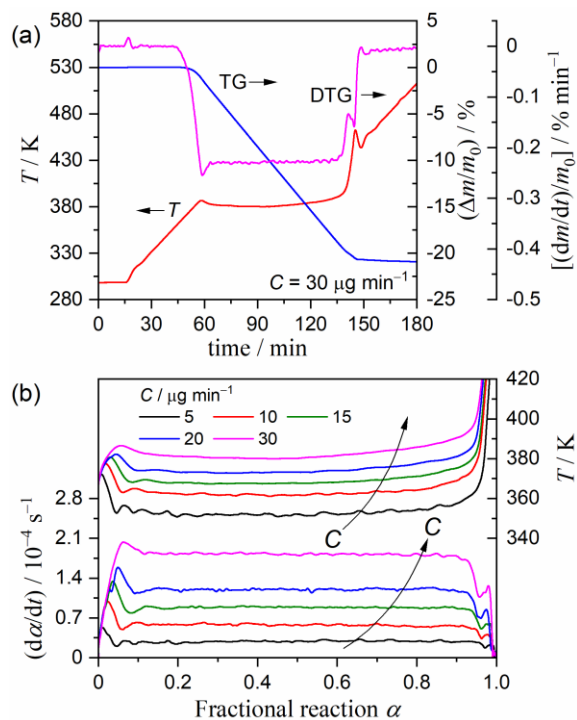


Figure S13. TG–DTG curves under CRTA conditions for the thermal dehydration of $\text{CaSO}_4 \cdot 2\text{H}_2\text{O}$ (approximately 15.0 mg) under the semi-closed conditions in a stream of N_2 gas (flowrate: $80 \text{ cm}^3 \text{ min}^{-1}$): (a) typical TG–DTG records and (b) temperature profile and transformation rate at various programmed C values.

(3) Isoconversional kinetic analysis

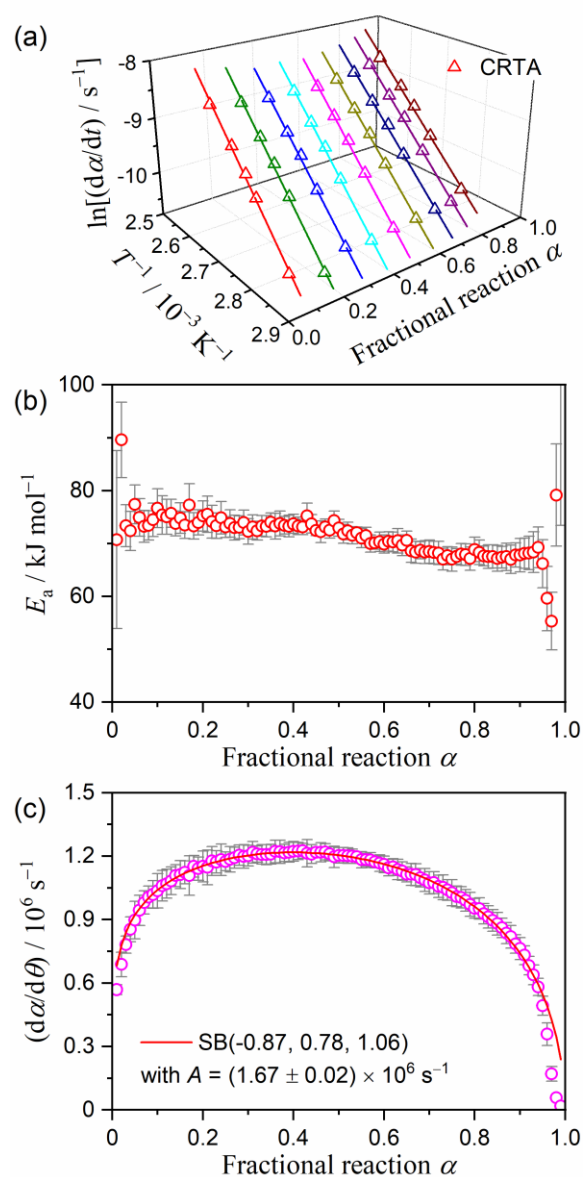


Figure S14. Isoconversional kinetic analysis for the thermal dehydration of $\text{CaSO}_4 \cdot 2\text{H}_2\text{O}$ recorded under CRTA conditions and semi-closed conditions in a stream of N_2 gas: (a) Friedman plots at different α values, (b) E_a values at different α values, and (c) experimental master plot of $(d\alpha/d\theta)$ versus α .

(4) Morphological changes

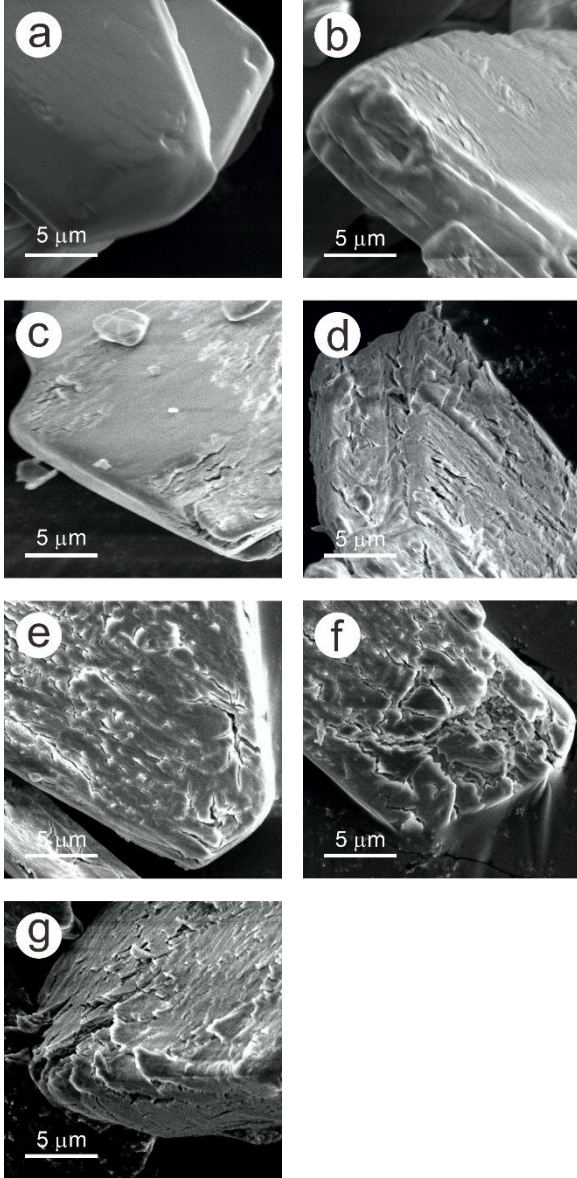


Figure S15. SEM images of the sample dehydrated partially to different α values by heating nonisothermally at a β of 3 K min^{-1} under the same conditions as those for the kinetic data measurements for $\text{CaSO}_4 \cdot 2\text{H}_2\text{O}$ (approximately 15.0 mg) under the semi-closed conditions: (a) $\alpha = 0.01$ (370 K), (b) $\alpha = 0.04$ (390 K), (c) $\alpha = 0.13$ (403 K), (d) $\alpha = 0.53$ (420 K), (e) $\alpha = 0.81$ (430 K), (f) $\alpha = 0.98$ (443 K), and (g) $\alpha = 0.99$ (480 K).

■ Weibull function

$$F(t) = a_0 \left(\frac{a_3 - 1}{a_3} \right)^{\frac{1-a_3}{a_3}} \left\{ \frac{t - a_1}{a_2} + \left(\frac{a_3 - 1}{a_3} \right)^{\frac{1}{a_3}} \right\}^{a_3 - 1} \times \exp \left[- \left\{ \frac{t - a_1}{a_2} + \left(\frac{a_3 - 1}{a_3} \right)^{\frac{1}{a_3}} \right\}^{a_3} + \frac{a_3 - 1}{a_3} \right] \quad (\text{S1})$$

where a_0 is the amplitude, a_1 is the center, a_2 is the width, and a_3 is the shape parameters.

(5) Mathematical deconvolution analysis

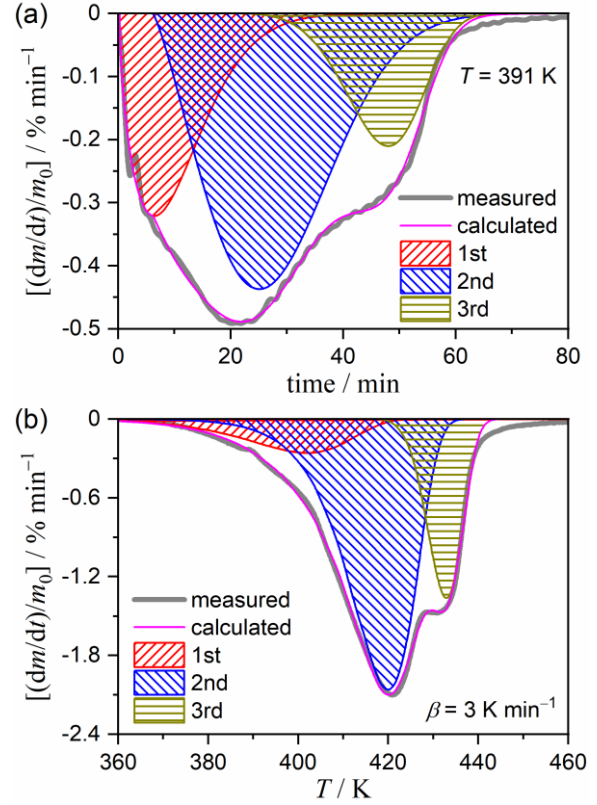


Figure S16. Typical results of MDA for the DTG peaks of the thermal dehydration of $\text{CaSO}_4 \cdot 2\text{H}_2\text{O}$ under the semi-closed conditions: (a) at a constant temperature of 391 K (lower temperature) and (b) at a β of 3 K min^{-1} (higher temperature).

Table S4. Results of kinetic analysis for the component reaction steps using MDA for the thermal dehydration of $\text{CaSO}_4 \cdot 2\text{H}_2\text{O}$ under the semi-closed conditions

Temperature region	<i>i</i>	<i>c_i</i>	<i>E_{a,i}</i> / kJ mol ⁻¹	$\frac{d\alpha_i}{d\theta_i} = A_i f(\alpha_i)$ with $f(\alpha_i) = \alpha_i^{m_i} (1 - \alpha_i)^{n_i} [-\ln(1 - \alpha_i)]^{p_i}$					R ²
				<i>A_i</i> / s ⁻¹	<i>m_i</i>	<i>n_i</i>	<i>p_i</i>		
Lower temp. (Isothermal, 383 ≤ <i>T</i> ≤ 402)	1	0.25 ± 0.01	81.2 ± 6.6	(1.56 ± 0.03) × 10 ⁸	-0.56 ± 0.13	1.15 ± 0.05	0.91 ± 0.12	0.9993	
	2	0.56 ± 0.01	88.7 ± 1.7	(1.22 ± 0.01) × 10 ⁹	0.13 ± 0.02	0.97 ± 0.01	0.45 ± 0.02	0.9999	
	3	0.19 ± 0.02	70.7 ± 4.5	(6.87 ± 0.01) × 10 ⁶	-0.03 ± 0.01	1.01 ± 0.01	0.80 ± 0.01	0.9999	
Higher temp. (Nonisothermal, β ≥ 2 K min ⁻¹)	1	0.14 ± 0.02	77.7 ± 1.2	(5.62 ± 0.02) × 10 ⁷	-0.24 ± 0.02	1.04 ± 0.01	0.54 ± 0.02	0.9999	
	2	0.65 ± 0.03	66.0 ± 7.9	(1.15 ± 0.01) × 10 ⁶	0.23 ± 0.02	0.94 ± 0.01	0.37 ± 0.01	0.9999	
	3	0.21 ± 0.01	54.1 ± 0.9	(4.63 ± 0.01) × 10 ⁴	0.20 ± 0.01	0.97 ± 0.01	0.52 ± 0.01	0.9999	

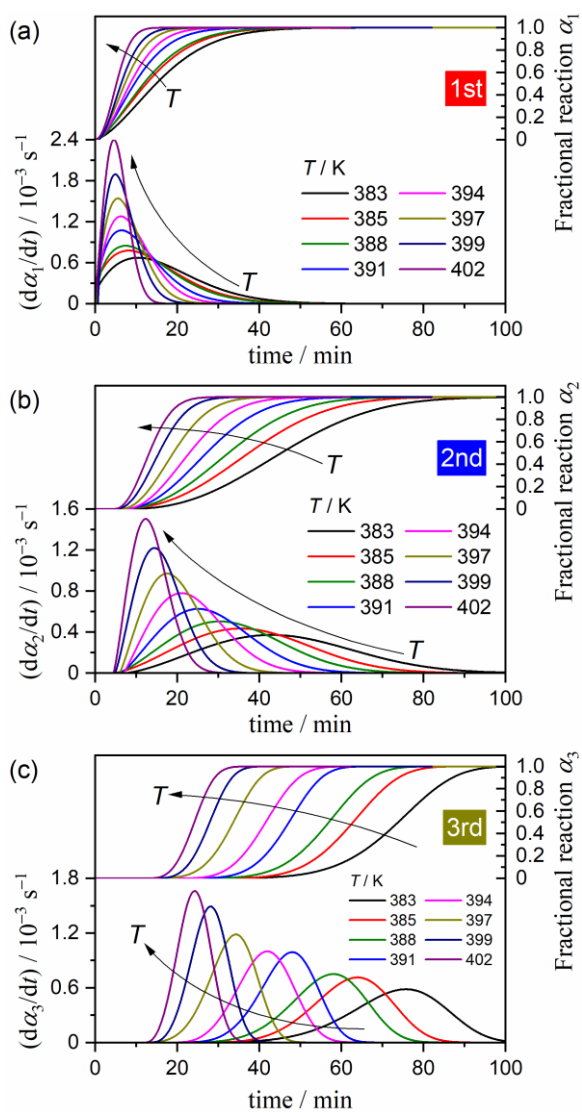


Figure S17. Series of kinetic curves for each reaction step i at different constant temperatures in the lower-temperature region, as obtained by MDA: (a) $i=1$, (b) $i=2$, and (c) $i=3$.

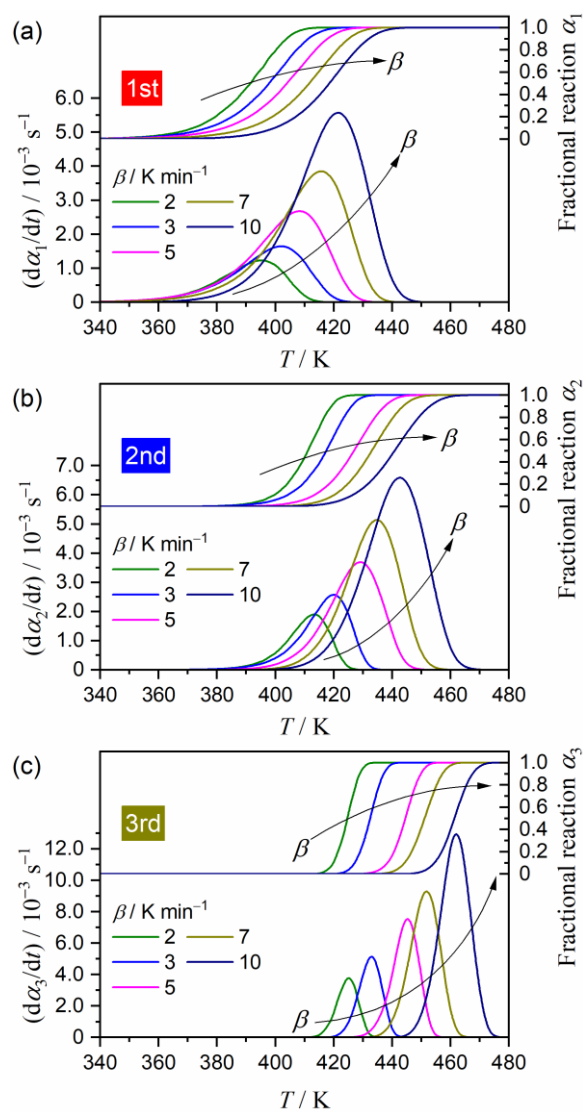


Figure S18. Series of kinetic curves for each reaction step i at different β values in the higher-temperature region, as obtained by MDA: (a) $i=1$, (b) $i=2$, and (c) $i=3$.

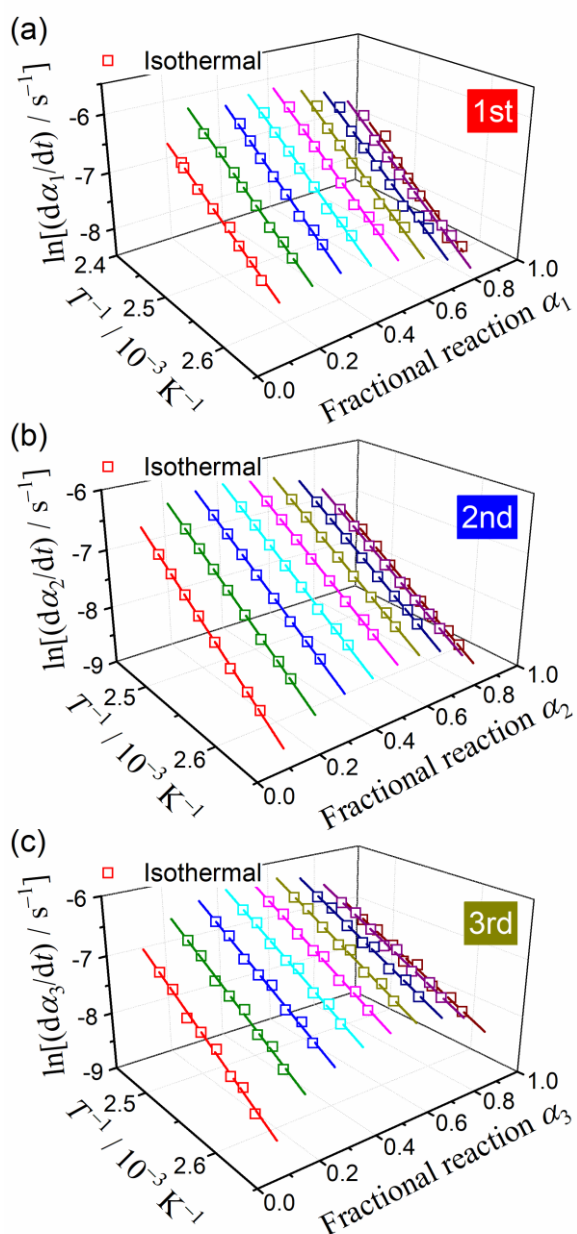


Figure S19. Friedman plots at various α_i values for the mathematically separated kinetic data at various constant temperatures in the lower-temperature region: (a) $i = 1$, (b) $i = 2$, and (c) $i = 3$.

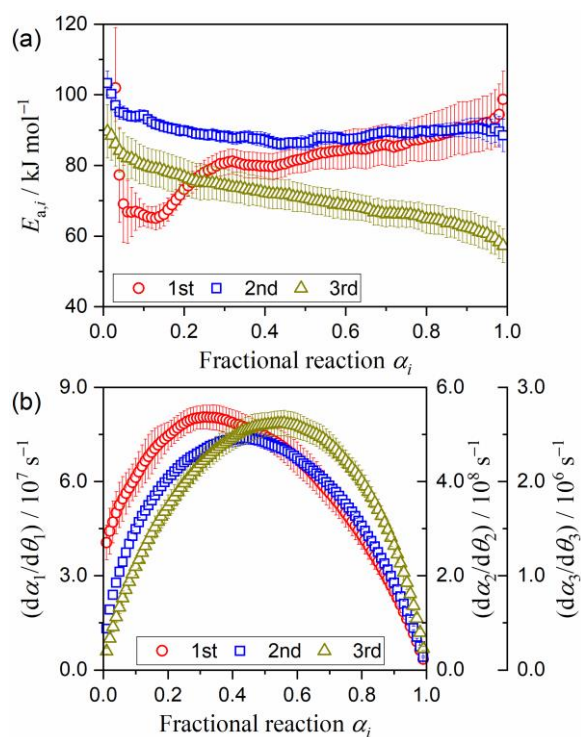


Figure S20. Results of the isoconversional kinetic analysis applied to the mathematically separated kinetic data at various constant temperatures in the lower-temperature region: (a) E_a values at various α_i values and (b) experimental master plots of $d\alpha_i/d\theta_i$ versus α_i .

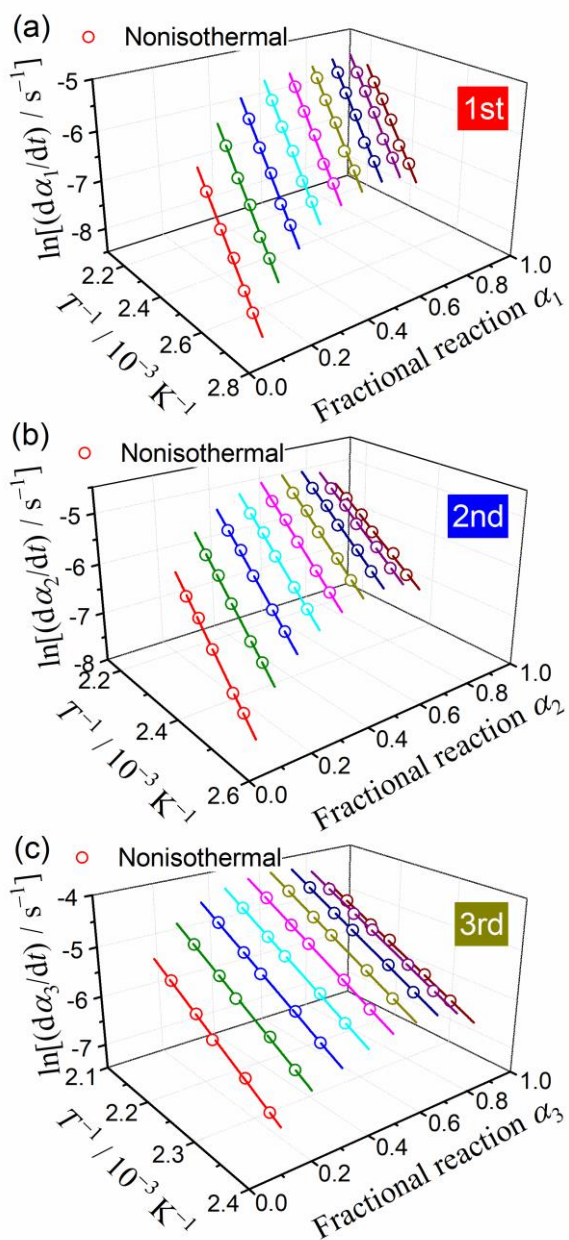


Figure S21. Friedman plots at various α_i values for the mathematically separated kinetic data at various β values in the higher-temperature region: (a) $i = 1$, (b) $i = 2$, and (c) $i = 3$.

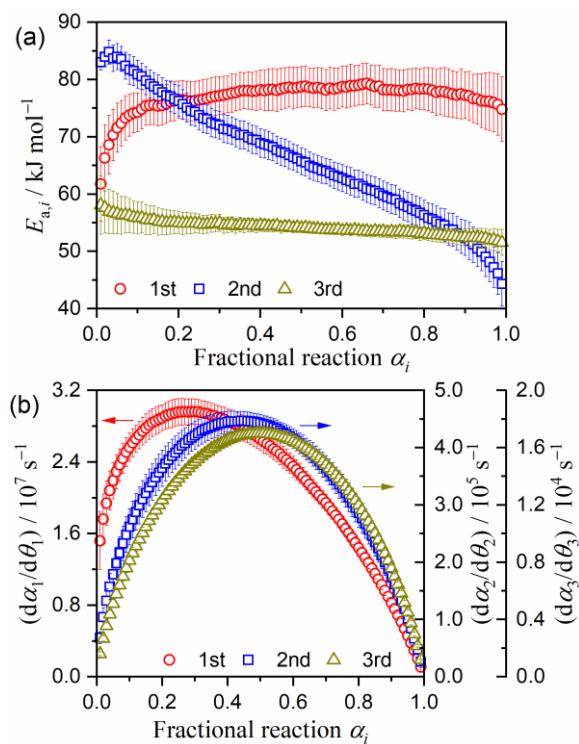


Figure S22. Results of the isoconversional kinetic analysis applied to the mathematically separated kinetic data at various β values in the higher-temperature region: (a) E_a values at various α_i values and (b) experimental master plots of $d\alpha_i/d\theta_i$ versus α_i .